iJRASET
International Journal For Research in Applied Science and Engineering Technology

INTERNATIONAL JOURNAL FOR RESEARCH
IN APPLIED SCIENCE & ENGINEERING TECHNOLOGY

Volume: 14 Issue: IX Month of publication: September 2026

DOI: https://doi.org/10.22214/ijraset.2026.84869

www.ijraset.com

Call: 08813907089 | E-mail ID: ijraset@gmail.com

International Journal for Research in Applied Science & Engineering Technology (IJRASET)
ISSN: 2321-9653; IC Value: 45.98; SJ Impact Factor: 7.538
Volume 14 Issue IX Sep 2026- Available at www.ijraset.com

Physics-Informed Hybrid ANN-P&O Optimal-Flux Control for Energy-Efficient Induction Motor Drives

Tan Minh Le
[1]Faculty of Electrical and Electronics, Thu Duc College of Technology, Ho Chi Minh City, Vietnam

Abstract: This paper proposes a physics-informed hybrid artificial neural network (ANN) and perturb-and-observe (P&O) optimal-flux controller for reducing losses in a field-oriented induction motor drive. The ANN rapidly estimates the optimal rotor-flux reference from measured operating variables, and a bounded P&O search locally refines this estimate using averaged input power. Paired MATLAB/Simulink simulations under a common 20 s operating profile show that the proposed controller reduces average loss power and input energy relative to constant-flux field-oriented control while maintaining low steady-state flux-command ripple. A coefficient-sensitivity study indicates positive calculated energy savings across the evaluated core-loss range. The results are limited to simulation; experimental parameter identification and hardware validation remain necessary.
Keywords: Artificial neural network, field-oriented control, induction motor, loss-minimization control, optimal rotor flux, perturb and observe.

I. INTRODUCTION

Induction motors are widely used in industrial applications because of their simple construction, low cost, and high reliability. However, their energy efficiency is often suboptimal, especially under partial-load conditions, leading to considerable energy waste [1]–[3]. Field-oriented control (FOC) has become the standard for high-performance drives, but conventional FOC maintains a constant rotor flux at the rated value, which causes excessive iron and copper losses when the motor operates at light loads [4], [5].

Loss-minimization control (LMC) has been extensively studied to address this issue. Model-based LMC methods rely on sufficiently accurate motor and loss parameters [5], [9]-[11], and their performance can deteriorate when those parameters change with temperature or magnetic saturation. Search-based methods such as perturb and observe (P&O) are less dependent on a detailed loss model, but they commonly exhibit slow convergence and steady-state oscillation [12]. More recently, artificial-intelligence techniques, including neural networks and reinforcement learning, have been applied to online flux optimization [6]-[8], [14]-[17]. Nevertheless, purely data-driven methods require representative training data and may not adapt reliably to operating conditions outside the training domain.

To address these complementary limitations, this paper proposes a physics-informed hybrid ANN-P&O controller embedded in an indirect rotor-flux-oriented control system. The ANN provides a rapid operating-point flux estimate learned from constrained loss-model targets, whereas bounded P&O supplies a small online correction using an augmented DC-link input-power objective. The method is designed to retain the ANN's fast response while limiting the search range and steady-state flux ripple. The main contributions are as follows:

1) Generation of a constrained optimal rotor-flux target from a loss model that includes stator copper, rotor copper, and iron losses;
2) Development of a four-input ANN predictor using [omega_m, T_e, i_d, i_q], with one 64-neuron hidden layer and a tanh activation function;
3) Integration of a bounded adaptive P&O optimizer that minimizes 50 ms averaged total input power, applies a torque-dependent lower flux bound, and includes ANN-output filtering and a flux-rate limiter; and
4) Paired MATLAB/Simulink R2024b evaluation under a common operating profile, together with ANN test results of RMSE = 0.01918 Wb, MAE = 0.01107 Wb, and R = 0.99205.

The remainder of this paper is organized as follows. Section II presents the induction-motor model and loss components. Section III describes the proposed physics-informed hybrid ANN-P&O optimizer. Section IV defines the simulation setup and data-generation procedure. Section V presents and discusses the simulation and ANN-validation results. Section VI concludes the paper.

International Journal for Research in Applied Science & Engineering Technology (IJRASET)
ISSN: 2321-9653; IC Value: 45.98; SJ Impact Factor: 7.538
Volume 14 Issue IX Sep 2026- Available at www.ijraset.com

II. MATHEMATICAL MODEL OF INDUCTION MOTOR INCLUDING LOSSES

A. Induction Motor Model in Different Reference Frames

The three-phase induction motor is first described in the natural abc reference frame. To simplify control, it is transformed to the stationary $\alpha\beta$ frame (Clarke transformation) and then to the synchronously rotating dq frame (Park transformation). Under the rotor-field-oriented condition, the rotor flux is aligned with the d-axis ($\psi_{rq} = 0$).

The stator voltage equations in the dq frame are [10], [11]:

$$u_{sd} = R_s i_{sd} + \frac{d\psi_{sd}}{dt} - \omega_e \psi_{sq} \tag{1}$$

$$u_{sq} = R_s i_{sq} + \frac{d\psi_{sq}}{dt} + \omega_e \psi_{sd} \tag{2}$$

where

u_{sd}, u_{sq} – stator voltages (V),
i_{sd}, i_{sq} – stator currents (A),
ψ_{sd}, ψ_{sq} – stator fluxes (Wb),
R_s – stator resistance (Ω),
ω_e – synchronous angular speed (rad/s).

The rotor flux dynamics are given by:

$$\psi_{rd} = \frac{L_m}{1+T_r p} i_{sd}, T_r = \frac{L_r}{R_r} \tag{3}$$

$$\omega_{sl} = \frac{L_m i_{sq}}{T_r \psi_{rd}}, \omega_e = \omega_r + \omega_{sl} \tag{4}$$

where:

L_m – magnetizing inductance (H),
L_r – rotor inductance (H),
R_r – rotor resistance (Ω),
T_r – rotor time constant (s),
$p = d/dt$ – differential operator,
ω_{sl} – slip speed (rad/s),
ω_r – rotor mechanical speed (rad/s).

The electromagnetic torque is:

$$T_e = \frac{3}{2} p \frac{L_m}{L_r} \psi_{rd} i_{sq} \tag{5}$$

with p the number of pole pairs.

B. Loss Components and Their Relationship with Rotor Flux

The total power loss in the induction motor consists of stator copper loss, rotor copper loss, and iron loss [5], [10]:

$$P_{\text{loss}} = P_{\text{Cu},s} + P_{\text{Cu},r} + P_{\text{Fe}} \tag{6}$$

The copper losses are expressed as:

$$P_{\text{Cu},s} = \frac{3}{2} R_s (i_{sd}^2 + i_{sq}^2), P_{\text{Cu},r} = \frac{3}{2} R_r i_r^2 \tag{7}$$

The iron loss is approximated by:

$$P_{\text{Fe}} = \frac{1.5(\omega_e \psi_{rd})^2}{R_{Fe}} \tag{8}$$

where R_{Fe} is an equivalent resistance representing iron losses (hysteresis and eddy currents) [9], [10].

By substituting $i_{sq} = \frac{2T_e L_r}{3pL_m \psi_{rd}}$ into (7) and (8), the total loss becomes a convex function of ψ_{rd} [5], [9]:

$$P_{\text{loss}}(\psi_{rd}) = K_1 \psi_{rd}^2 + K_2 / \psi_{rd}^2 \tag{9}$$

International Journal for Research in Applied Science & Engineering Technology (IJRASET)
ISSN: 2321-9653; IC Value: 45.98; SJ Impact Factor: 7.538
Volume 14 Issue IX Sep 2026- Available at www.ijraset.com

where K_1 and K_2 depend on motor parameters and the operating torque. This function has a unique minimum at an optimal rotor flux $\psi_{rd,\text{opt}}$. When the load torque decreases, the optimal flux shifts to a lower value, which is the key principle behind loss-minimizing control.

C. Field-Oriented Control and Loss Minimization Principle

The block diagram of the indirect FOC system is shown in Fig. 1 (conceptually). The speed error is fed to a PI controller that generates the q-axis current reference:

$$i_{sq}^* = K_{p\omega}(\omega_r^* - \omega_r) + K_{i\omega}\int (\omega_r^* - \omega_r)dt \tag{10}$$

The d-axis current reference is derived from the desired rotor flux reference ψ_r^*:

$$i_{sd}^* = \frac{\psi_r^*}{L_m} \tag{11}$$

Two PI current controllers produce the voltage references u_{sd}^* and u_{sq}^* in the rotating frame. These are transformed back to the stationary abc frame and then to PWM signals for the inverter.

In conventional FOC, the rotor flux is kept constant at its rated value $\psi_{r,\text{rated}}$. At light loads, this leads to unnecessarily high iron losses (due to high flux) and also increases copper losses because the magnetizing current is maintained at a high level. By reducing the flux when the load is low, both iron and copper losses can be reduced, as indicated by (9). However, the optimal flux is not fixed but varies with load torque and speed, requiring an adaptive online optimizer.

III. PROPOSED HYBRID ANN–P&O ROTOR FLUX OPTIMIZATION STRATEGY

A. Principle of the Proposed Method

The proposed optimizer uses the state vector x = [omega_m, T_e, i_d, i_q]^T. During offline preparation, the target flux psi_r,opt is obtained by minimizing the modeled total loss over a bounded flux interval. During online operation, the ANN predicts this target and a bounded P&O search applies a small local correction.

$$\psi_{r,\text{opt}} = \arg\min_{0.30\le\psi\le0.96} P_{\text{loss}}(\psi, \omega_m, T_e) \tag{12}$$

The workflow comprises four stages: (i) physics-informed target generation, (ii) ANN training and weight export, (iii) analytical or measured loss estimation, and (iv) bounded P&O refinement around the ANN estimate.

B. Physics-Informed ANN Training

Training data are generated from Simulink logs DATA = [omega_m, T_e, i_d, i_q, P_loss]. The measured loss used for data conditioning is computed from the power balance:

$$P_{\text{loss}} = 1.5(v_d i_d + v_q i_q) - T_e\omega_m \tag{13}$$

For target generation, the constrained loss model is minimized over the rotor-flux grid. The ANN learns the mapping x -> psi_r,opt, where x = [ω_m, T_e, i_d, i_q]^T.

$$P_{\text{loss}}(\psi) = P_{\text{Cu},s} + P_{\text{Cu},r} + P_{\text{Fe}} \tag{14}$$

The implemented ANN has four physical-unit inputs [ω_m, T_e, i_d, i_q], one hidden layer with 64 neurons and tanh activation, and one scalar output. The dataset is not pre-normalized in prepare_dataset.m. Instead, train_ai.m stores ps_xmin and ps_xmax so that the Simulink block applies the same min-max normalization during online inference. After training on 99,894 samples, the held-out test set produced RMSE = 0.01918 Wb, MAE = 0.01107 Wb, and R = 0.99205.

C. Online Loss Estimation

The online P&O cost is the total input-power estimate formed from the measured DC-link power and an explicit core-loss term:

$$P_{\text{in,total}} = P_{\text{in,dc}} + P_{\text{Fe}} \tag{15}$$

International Journal for Research in Applied Science & Engineering Technology (IJRASET)
ISSN: 2321-9653; IC Value: 45.98; SJ Impact Factor: 7.538
Volume 14 Issue IX Sep 2026- Available at www.ijraset.com

The Specialized Power Systems induction-machine block does not explicitly parameterize iron loss. Consequently, the online objective augments measured DC-link input power with the core-loss estimate defined below. The same objective definition is applied to all controllers and in post-processing.

$$P_{\mathrm{Fe}} = 1.5(K_h|\omega_e| + K_e\omega_e^2)(L_m i_d)^2 \tag{16}$$

The measured ANN inputs are low-pass filtered with a 10 ms time constant, and the ANN flux output is filtered with a 30 ms time constant. The augmented input-power signal is averaged over a 50 ms window before each P&O decision. Logged signals are decimated for storage at 100 microseconds, whereas the controller retains a 2 microsecond fixed step.

D. Bounded Adaptive P&O Refinement

At each 50 ms optimization update, Delta P_in = P_in(k) - P_in(k-1) is evaluated. If the input power increases following a perturbation, the search direction is reversed.

$$d(k+1) = \begin{cases} -d(k), & \Delta P_{\mathrm{in}} > 0 \\ d(k), & \text{otherwise} \end{cases} \tag{17}$$

The perturbation step is adaptive: 0.003 Wb for large power change, 0.0015 Wb for medium change, and 0.0005 Wb near the minimum.

$$\psi_{\mathrm{PO}}(k+1) = \psi_{\mathrm{PO}}(k) + d(k)\,\Delta\psi \tag{18}$$

E. Hybrid ANN-P&O Flux Optimization

The P&O search is constrained to psi_PO in [psi_ANN - 0.015, psi_ANN + 0.015] Wb. The final command is formed by blending the filtered ANN estimate and the bounded P&O candidate:

$$\psi_r^* = \beta\,\psi_{\mathrm{PO}} + (1-\beta)\,\psi_{\mathrm{ANN},f}, \quad \beta = 0.05 \tag{19}$$

F. Flux Saturation and Safety Constraints

The final flux reference is constrained by a torque-dependent lower bound: 0.20 Wb at light load, 0.35 Wb at medium load, and 0.65 Wb at heavy load. The upper bound is 0.96 Wb.

$$\varphi_{\min}(T_e) = \begin{cases} 0.20\ \mathrm{Wb}, & |T_e| < 50\ \mathrm{Nm} \\ 0.35\ \mathrm{Wb}, & 50 \le |T_e| < 120\ \mathrm{Nm} \\ 0.65\ \mathrm{Wb}, & \text{otherwise} \end{cases} \tag{20}$$

This formulation combines a physics-informed ANN estimate with a bounded local P&O correction. A 10 ms state filter and a 30 ms ANN-output filter attenuate switching-related ripple, while a 1 Wb/s rate limiter prevents abrupt flux commands from exciting the inner current and torque loops.

The online algorithm is executed as follows:

1) Read x = [omega_m, T_e, i_d, i_q]^T and the averaged total input-power estimate from the motor model.
2) Normalize x using the min-max parameters stored in weights_flux.mat.
3) Compute psi_ANN by forward propagation through the exported ANN weights.
4) Detect speed or torque changes and reset the P&O state to psi_ANN when a change is detected.
5) Every 50 ms, perform one adaptive P&O update using the variation in averaged total input power.
6) Constrain the P&O candidate to psi_ANN,f +/- 0.015 Wb.
7) Blend psi_PO with the filtered ANN estimate using beta = 0.05.
8) Rate-limit the flux command to 1 Wb/s and then constrain it to 0.20-0.96 Wb.

IV. SIMULATION SETUP

The controller was implemented in MATLAB/Simulink R2024b using fluxotpv1.slx with a 2 microsecond fixed step. Five controllers were evaluated in paired 20 s simulations with identical motor parameters, inverter settings, speed command, and load profile: constant-flux FOC, Loss Model Control, conventional P&O, ANN-only, and Hybrid ANN-P&O. The final light-load interval was extended from 7.2 s to 20 s to emphasize the operating region in which flux optimization is expected to provide the greatest benefit.

Measured DC-link power, mechanical output power, currents, torque, speed, and the applied flux command were logged. Because the machine block omits explicit core-loss parameterization, total input energy was evaluated by integrating P_in,dc + P_Fe. A +/-

International Journal for Research in Applied Science & Engineering Technology (IJRASET)
ISSN: 2321-9653; IC Value: 45.98; SJ Impact Factor: 7.538
Volume 14 Issue IX Sep 2026- Available at www.ijraset.com

20% coefficient-sensitivity analysis was applied to K_h and K_e. These coefficients require experimental identification before the results can be generalized to hardware.

The motor under study is a 50 HP, 460 V, 50 Hz three-phase squirrel-cage induction motor. The parameters used in the simulation and training scripts are listed in Table 1.

TABLE I
INDUCTION MOTOR SIMULATION PARAMETERS

Parameter	Value
Rated power	50 HP
Rated speed	1450 rpm
Rated voltage	460 V
Supply frequency	50 Hz
Stator resistance (Rs)	0.087 ohm
Rotor resistance (Rr)	0.228 ohm
Stator leakage inductance (Lls)	0.0001 H
Rotor leakage inductance (Llr)	0.0008 H
Mutual inductance (Lm)	0.0347 H
Moment of inertia (J)	0.662 kg.m2
Number of pole pairs (p)	2
Flux constraint	0.20-0.96 Wb

V. RESULTS AND DISCUSSION

All reported values were obtained from paired MATLAB/Simulink R2024b logs and the deployed ANN weights. Constant-flux FOC is used as the principal baseline because it represents conventional vector-control operation. All controllers were tested under the same 20 s speed-load profile, with the final low-load interval extended to evaluate the operating region in which optimal-flux control is expected to yield the largest energy benefit.

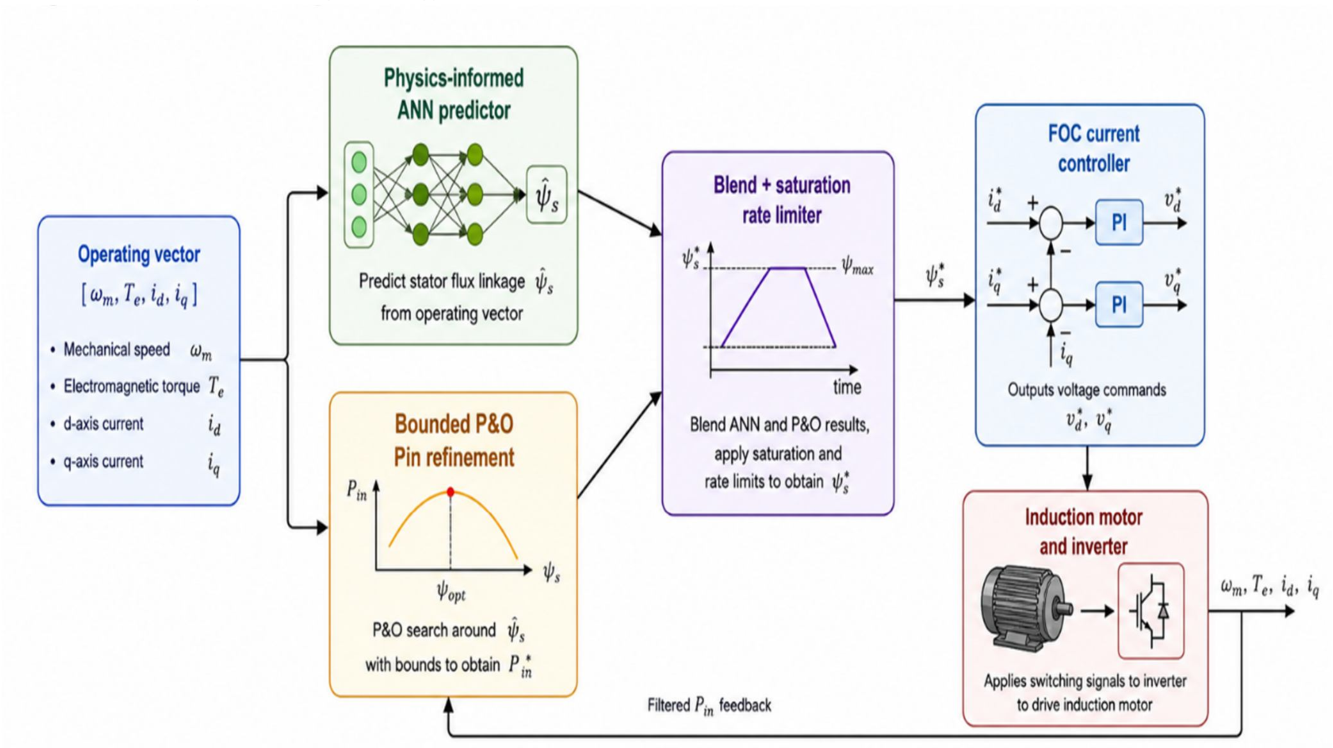

Fig. 1 Hybrid ANN-P&O architecture used in the indirect field-oriented induction-motor drive.

©IJRASET: All Rights are Reserved | SJ Impact Factor 7.538 | ISRA Journal Impact Factor 7.894 |

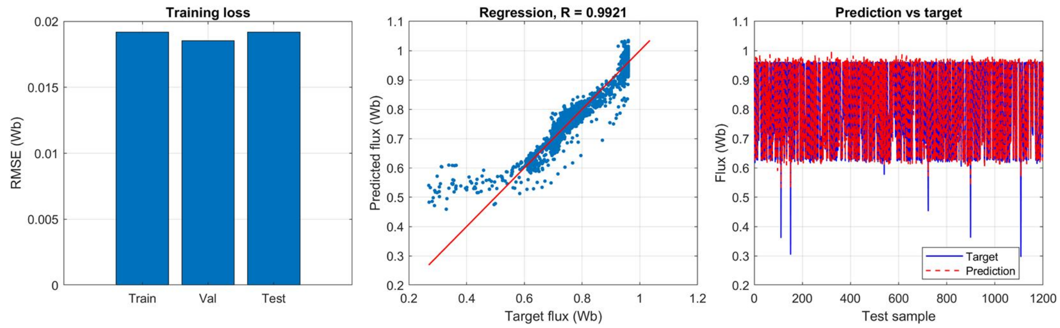

Fig. 2 ANN training performance: RMSE loss, test regression, and prediction versus target optimal flux.

On the held-out test set, the ANN achieved RMSE = 0.01918 Wb, MAE = 0.01107 Wb, MAPE = 1.5116%, R2 = 0.98416, and R = 0.99205. Relative to the 0.20-0.96 Wb admissible flux range, these results support using the ANN output as the center of the bounded P&O search window within the simulated operating domain.

TABLE II
ANN OPTIMAL-FLUX PREDICTION PERFORMANCE

Metric	Train	Validation	Test
RMSE (Wb)	0.01919	0.01853	0.01918
MAE (Wb)	0.01108	0.01091	0.01107
MAPE (%)	1.5235	1.4866	1.5116
R2	0.98428	0.98521	0.98416
R	0.99211	0.99258	0.99205

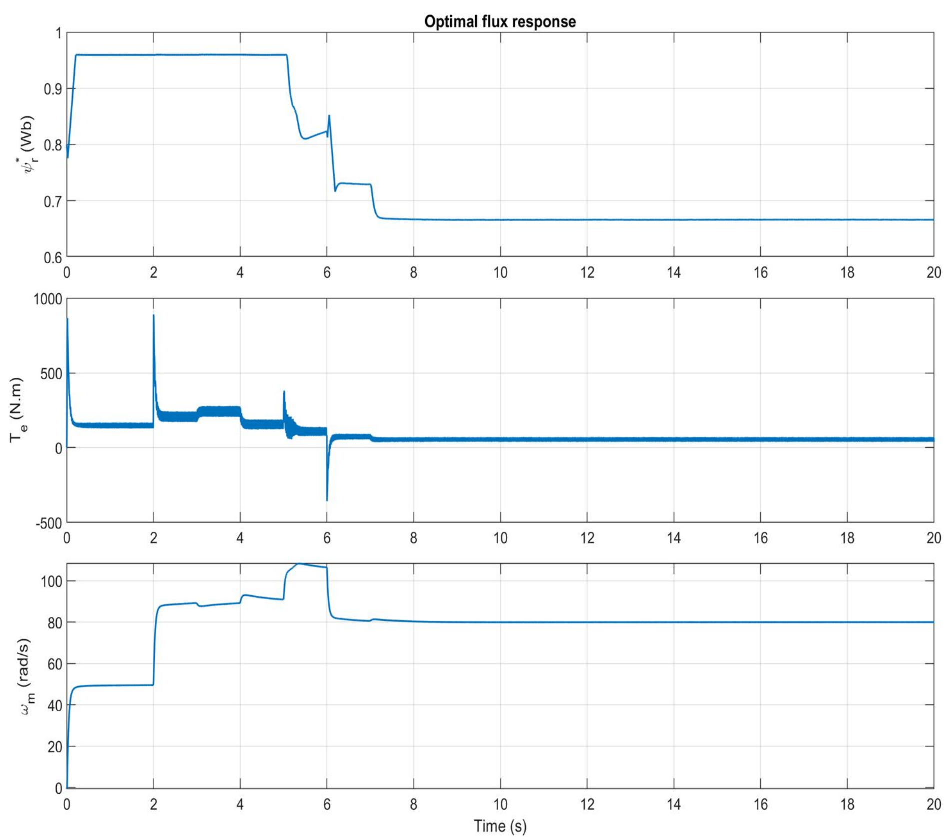

Fig. 3 Optimal flux response with load torque and speed under the multi-step operating profile.

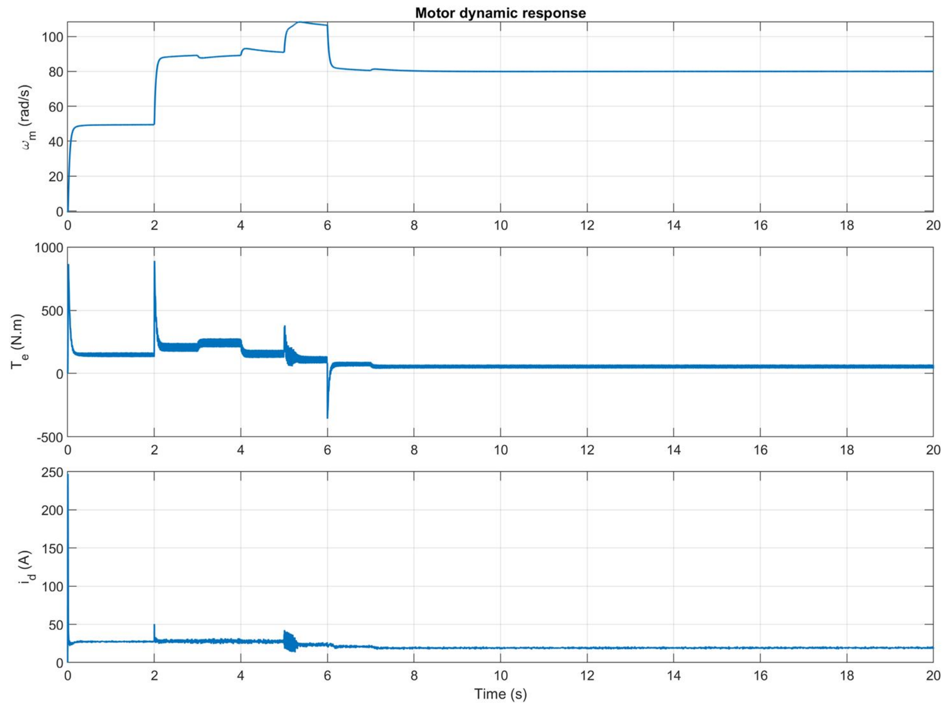

Fig. 4 Motor dynamic response: speed, electromagnetic torque, and d-axis current.

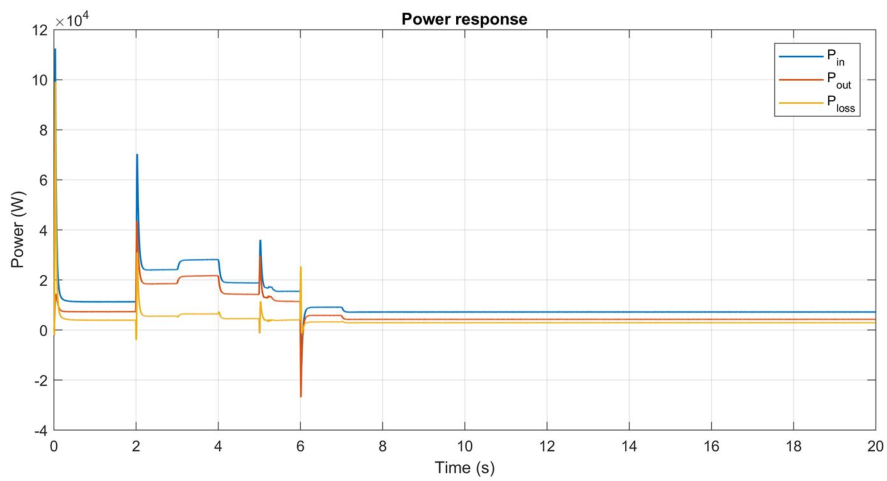

Fig. 5 Proposed-controller power response: measured DC-link input augmented by modeled core loss, mechanical output, and total loss.

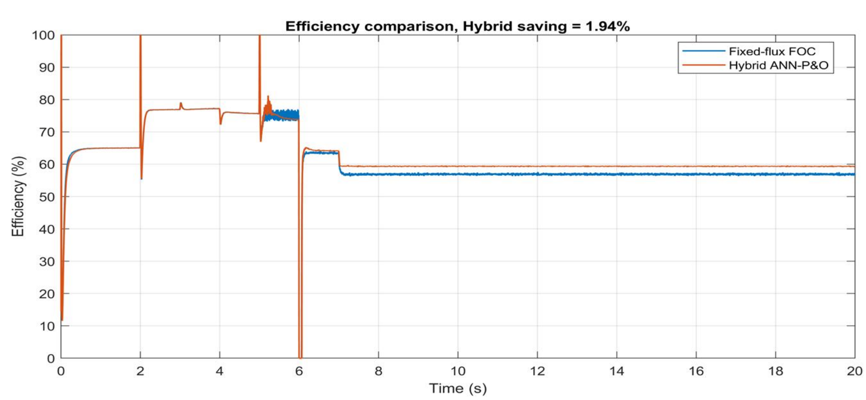

Fig. 6 Efficiency comparison between fixed-flux FOC and Hybrid ANN-P&O with integrated energy saving.

International Journal for Research in Applied Science & Engineering Technology (IJRASET)
ISSN: 2321-9653; IC Value: 45.98; SJ Impact Factor: 7.538
Volume 14 Issue IX Sep 2026- Available at www.ijraset.com

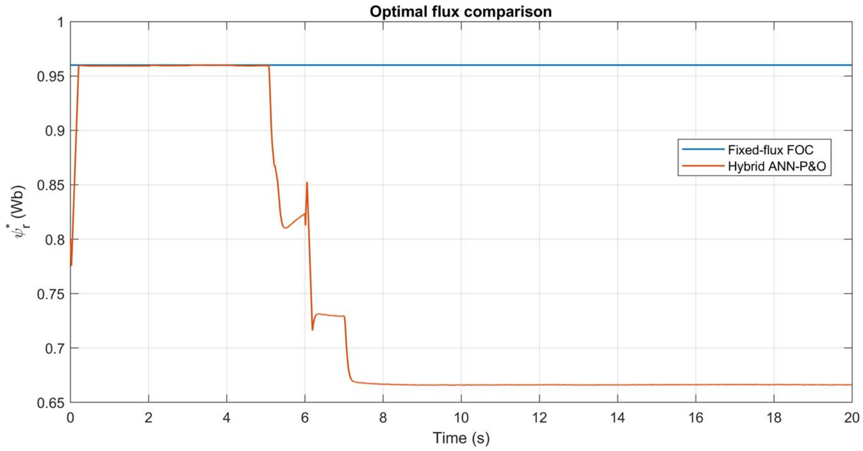

Fig. 7 Logged flux-command comparison after supervisory filtering and the 1 Wb/s rate limiter.

At high load, the flux remains near 0.96 Wb to preserve torque capability, and the energy difference from constant-flux FOC is below 0.03%. Over the 7.2-20 s light-load interval, the Hybrid controller reduces average d-axis current from 27.518 A to 19.145 A and yields 4.2707% input-energy saving. The corresponding efficiency increases from 56.888% to 59.341%.

Across the complete profile, average loss power decreases by 5.0528%, and average efficiency increases by 1.1205 percentage points. The integrated input energy, calculated using trapz(t, P_in), decreases from 61.993 Wh to 60.787 Wh, corresponding to a 1.9442% saving over the 20 s profile.

TABLE III
PAIRED CONTROLLER COMPARISON UNDER THE SAME 20 S PROFILE

Algorithm	Average Loss (W)	Efficiency (%)	Flux Ripple (Wb)	Settling Time (s)	Energy Saving (%)
Constant Flux	3943.80	64.657	0.00000	0.00000	0.00000
Loss Model Control	3716.70	65.986	0.11552	0.05630	2.0759
Conventional P&O	3921.99	64.712	0.00700	0.00000	0.39750
ANN-only	3743.90	65.782	0.00048	0.11970	1.9486
Hybrid ANN-P&O	3744.53	65.777	0.00063	0.12230	1.9442

TABLE IV
OVERALL IMPROVEMENT AGAINST CONSTANT-FLUX OPERATION

Metric	Constant Flux	Proposed	Relative Change
Average Input Power (W)	11158.63	10941.68	1.9442
Average Loss Power (W)	3943.80	3744.53	5.0528
Efficiency (%)	64.657	65.777	1.1205
Average id (A)	27.666	21.725	21.473
Average Flux (Wb)	0.96000	0.75154	21.714
Energy Consumption (Wh)	61.993	60.787	1.9442
Energy Saving (%)	0.00000	1.9442	1.9442

Loss Model Control, ANN-only, conventional P&O, and Hybrid ANN-P&O reduce input energy by 2.0759%, 1.9486%, 0.39750%, and 1.9442%, respectively, relative to constant-flux FOC. Thus, the Hybrid controller is not the best nominal-energy performer in this simulation; its energy result is essentially equal to ANN-only and slightly below Loss Model Control. The bounded P&O component is retained as a local online correction mechanism intended to address operating-point and parameter mismatch, but that robustness benefit requires dedicated mismatch tests and experimental validation.

Over the final 5 s steady-state window, the supervisory filters limit the Hybrid flux-command ripple to 0.00063 Wb, equivalent to 0.094% of its mean value. The measured 0.12230 s settling time is compatible with the slower efficiency-optimization loop and avoids imposing high-frequency flux-command variations on the inner FOC current loops.

Reducing flux lowers i_d and the modeled hysteresis and eddy-current terms, while maintaining torque requires i_q to increase from 19.128 A to 27.479 A during extended light-load operation. The net calculated benefit remains positive because the modeled core-loss reduction exceeds the associated copper-loss increase. When the core-loss coefficients are scaled from 0.8 to 1.2, the calculated full-profile saving ranges from 1.3381% to 2.5303%, and the light-load saving ranges from 3.0831% to 5.4020%. Relative to constant-flux FOC, the speed and torque deviations have RMSE values of 0.456 rad/s and 13.352 N m, respectively. These findings establish simulation feasibility, but they do not replace coefficient identification, repeated experimental trials, or hardware validation.

VI. CONCLUSION

This paper presented a physics-informed Hybrid ANN-P&O optimal-flux strategy for loss-minimizing field-oriented control of an induction motor drive. The method combines constrained loss-model target generation, rapid ANN-based flux prediction, bounded P&O refinement, input and output filtering, torque-dependent flux constraints, and flux-command rate limiting.

Under the paired MATLAB/Simulink R2024b simulations, the proposed controller reduced average loss power from 3943.80 W to 3744.53 W and increased average efficiency from 64.657% to 65.777% relative to constant-flux FOC. Input energy over the 20 s profile decreased by 1.9442%, and average d-axis current decreased from 27.666 A to 21.725 A. The filtered flux command exhibited 0.00063 Wb steady-state ripple and a 0.12230 s settling time.

The deployed ANN achieved test RMSE = 0.01918 Wb, MAE = 0.01107 Wb, MAPE = 1.5116%, R2 = 0.98416, and R = 0.99205. The controller's nominal energy saving was comparable to ANN-only and slightly lower than Loss Model Control; therefore, no claim of universal superiority is made. Future work should identify the loss coefficients experimentally, test parameter and measurement mismatch explicitly, compare computational burden, and validate the controller on a DSP- or FPGA-based drive platform.

REFERENCES

[1] R. Abdelati and M. F. Mimouni, "Optimal control strategy of an induction motor for loss minimization using Pontryaguin principle," European Journal of Control, vol. 49, pp. 94-106, 2019, doi: 10.1016/j.ejcon.2019.02.004.

[2] A. El Fadili, F. Giri, A. El Magri, R. Lajouad, and F. Z. Chaoui, "Towards a global control strategy for induction motor: Speed regulation, flux optimization and power factor correction," International Journal of Electrical Power & Energy Systems, vol. 43, no. 1, pp. 1082-1096, 2012, doi: 10.1016/j.ijepes.2012.05.022.

[3] A. El Fadili, F. Giri, A. El Magri, R. Lajouad, and F. Z. Chaoui, "Adaptive control strategy with flux reference optimization for sensorless induction motors," Control Engineering Practice, vol. 26, pp. 91-106, 2014, doi: 10.1016/j.conengprac.2013.12.005.

[4] D. H. Kim and K. Hirota, "Vector control for loss minimization of induction motor using GA-PSO," Applied Soft Computing, vol. 8, no. 4, pp. 1692-1702, 2008, doi: 10.1016/j.asoc.2006.09.001.

[5] S. Sujitjorn and K.-L. Areerak, "Numerical approach to loss minimization in an induction motor," Applied Energy, vol. 79, no. 1, pp. 87-96, 2004, doi: 10.1016/j.apenergy.2003.11.001.

[6] A. Arias, L. Romeral, E. Aldabas, and M. Jayne, "Stator flux optimised Direct Torque Control system for induction motors," Electric Power Systems Research, vol. 73, no. 3, pp. 257-265, 2005, doi: 10.1016/j.epsr.2004.06.014.

[7] K. Rai, S. B. L. Seksena, and A. Thakur, "A Golden Section Search Algorithm Based Loss Minimization for Induction Motor Drive," International Journal on Electrical Engineering and Informatics, vol. 11, no. 1, pp. 159-177, 2019, doi: 10.15676/ijeei.2019.11.1.9.

[8] C. Chen, H. Yu, F. Gong, and H. Wu, "Induction Motor Adaptive Backstepping Control and Efficiency Optimization Based on Load Observer," Energies, vol. 13, no. 14, Art. no. 3712, 2020, doi: 10.3390/en13143712.

[9] F. Tazerart, Z. Mokrani, D. Rekioua, and T. Rekioua, "Direct torque control implementation with losses minimization of induction motor for electric vehicle applications with high operating life of the battery," International Journal of Hydrogen Energy, vol. 40, no. 39, pp. 13827-13838, 2015, doi: 10.1016/j.ijhydene.2015.04.052.

[10] S. Karpe, S. A. Deokar, and A. M. Dixit, "Switching losses minimization by using direct torque control of induction motor," Journal of Electrical Systems and Information Technology, vol. 4, no. 2, pp. 225-242, 2017, doi: 10.1016/j.jesit.2016.08.007.

[11] L. M. Phuong, L. D. Dung, N. V. Thuyen, and N. H. Phong, "Real-time loss minimization control in induction machines based on DSP TMS320LF2812," Science & Technology Development Journal, vol. 16, no. K4, pp. 5-15, 2013.

[12] B. Hima Deepthi, P. Srinivasa Varma, M. Kiran Kumar, and K. V. Govardhan Rao, "An Enhanced Loss Model Based Online Flux Optimization Technique for Vector-Controlled Induction Motor Drives Including Leakage Inductance," International Journal of Electrical and Electronics Research, vol. 14, no. 1, pp. 110-122, 2026, doi: 10.37391/ijeer.140112.

[13] S. S. Sivaraju, T. Senthilkumar, R. Sankar, T. Anuradha, S. Usha, and I. B. Musirin, "Improving the efficiency of induction motor drive by flux and torque control: A hybrid LSE-RERNN approach," ISA Transactions, vol. 147, pp. 215-226, 2024, doi: 10.1016/j.isatra.2024.01.034.

[14] R. C. B. Rego, C. A. Diniz, J. J. Eckert, and L. C. A. Silva, "An adaptive unscented Kalman Filter with nonlinear model predictive control based on reinforcement learning for the induction motor control in electric vehicles," Engineering Applications of Artificial Intelligence, 2026, doi: 10.1016/j.engappai.2026.115363.

[15] U. K. Potnuru, S. K. Teegala, L. R. Kalabarige, V. Ippili, and M. R. Holla, "Dataset for optimized design parameters of three-phase induction motors with validation through machine learning," Data in Brief, vol. 63, Art. no. 112274, 2025, doi: 10.1016/j.dib.2025.112274.

[16] A. D Amico, S. Longo, M. Cellura, M. Caruso, and R. Miceli, "Environmental benefits and impacts forecasting for three-phase induction motors operations in marine applications: A multiple linear regression approach," Energy Reports, 2026, doi: 10.1016/j.egyr.2025.12.025.

[17] A. Kalinov, V. Melnykov, M. Z. Qawaqzeh, M. Zagirnyak, A. Szczesny, and E. Korzeniewska, "The methods and systems of Fault-Tolerant frequency vector control of induction motors in case of the stator circuit damage," International Journal of Electrical Power & Energy Systems, 2025, doi: 10.1016/j.ijepes.2025.110974.

[18] A. Kasri, K. Ouari, Y. Belkhier, D. Ziane, M. F. Benkhoris, and M. Benbouzid, "Optimized voltage vector selection for dual-star induction motor: Robust predictive direct torque control-based hysteresis-free approach," ISA Transactions, 2025, doi: 10.1016/j.isatra.2025.09.015.

BIOGRAPHIES OF AUTHORS

	**Tan Minh Le** was born in Tien Giang, Vietnam, in 1990. He received the B.Eng. and M.Eng. degrees in Electrical Engineering from Ho Chi Minh City University of Technology and Education, Vietnam, in 2014 and 2016, respectively. He is currently a lecturer with the Faculty of Electrical and Electronics Engineering, Thu Duc College of Technology, Ho Chi Minh City, Vietnam. His research interests include power systems operation, renewable energy, smart grids, and power system optimization. He can be contacted at email: tanleminh11@gmail.com

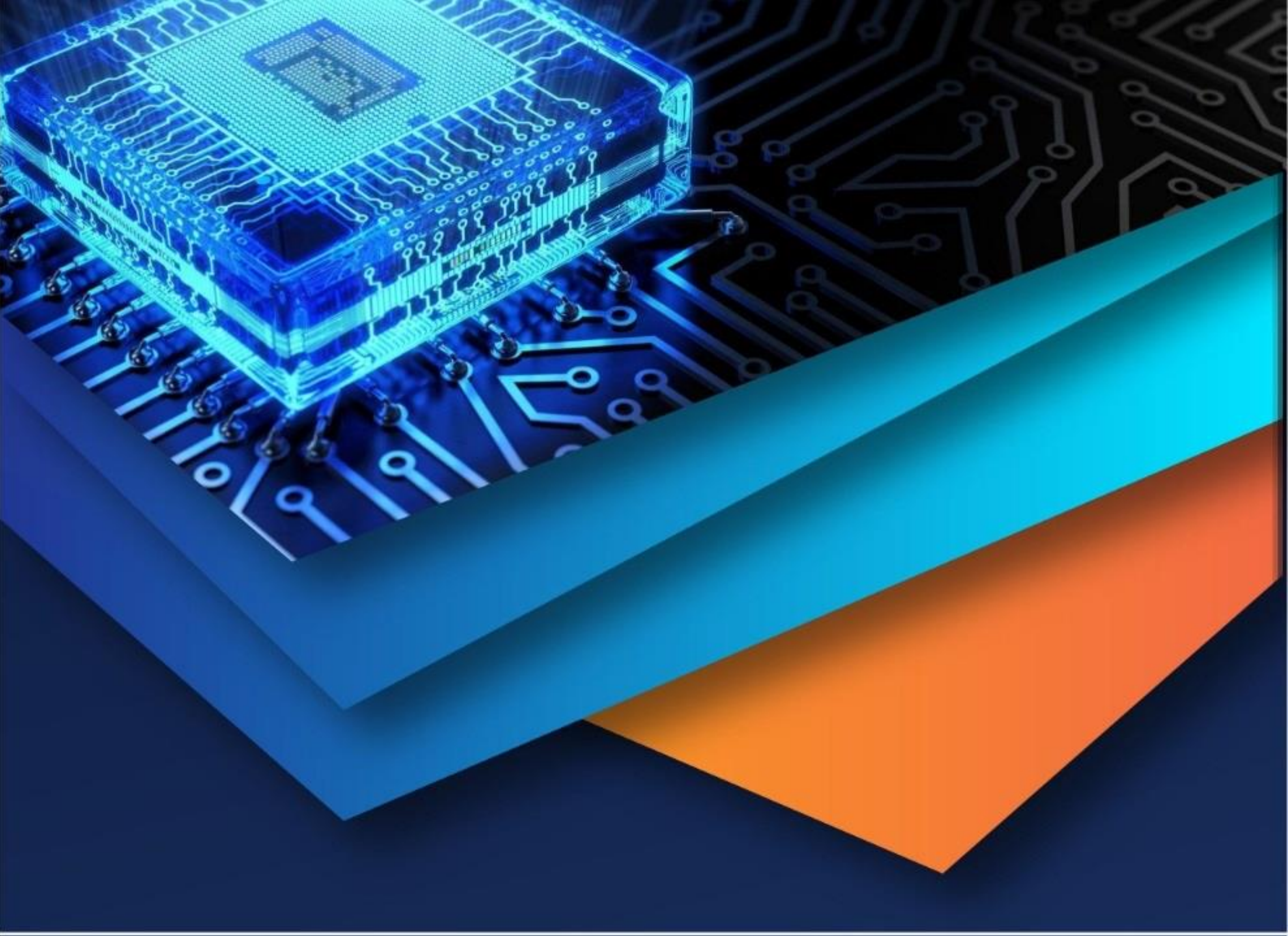

10.22214/IJRASET

45.98

IMPACT FACTOR: 7.129

IMPACT FACTOR: 7.429

INTERNATIONAL JOURNAL FOR RESEARCH

IN APPLIED SCIENCE & ENGINEERING TECHNOLOGY

Call : 08813907089 (24*7 Support on Whatsapp)